NUMERICAL STUDY OF MIXED CONVECTION AND ENTROPY GENERATION IN THE POISEULLE-BENARD CHANNEL IN DIFFERENT ANGLES

by

Mostafa NOUROLLAHI, Mousa FARHADI*, and Kurosh SEDIGHI

Babol University of Technology, Faculty of Mechanical Engineering,
Babon, Islamic Republic of Iran

Original scientific paper
UDC: 532.521/.528:536.24
DOI: 10.2298/TSCI1002329N

The issue of entropy generation and Nusselt number in Poiseuille-Benard channel flow are analyzed by solving numerically Navier-Stokes and energy equations with the use of the classic Boussinesq incompressible approximation. The Nusselt number is studied as a function of θ. In addition variations of entropy generation and the Bejan number as a function of θ and φ are studied. The channel angle (θ) and irreversibility (φ) were changed from –25 to 30 and from 10^{-5} to 1, respectively, whereas Reynolds, Peclet, and Rayleigh numbers were fixed at Re = 10, Pe = 20/3, and Ra = 10^4. More over the positive and negative effect of buoyancy force on flow field, Nusselt number and entropy generation are discussed. Optimum angle for different irreversibilities are specified by definition η as the rate of the Nusselt number to the entropy generation, the optimum angle was distinguished for different irreversibility. Results show that the Nusselt number changes very slightly and is almost constant when θ changes from –10 to 10 and the Nusselt number decreases sharply when θ increases from 20 to 30 or decreases from –15 to –25. Moreover it has been found that the entropy generation due to heat transfer is localized at areas where heat exchanged between the walls and the flow is maximum, while the entropy generation due to fluid friction is maximum at areas where the velocity gradients are maximum such as vortex centers. Consequently when θ is decreased from –15 to –25 or is increased from 20 to 30 entropy generation for small irreversibilities decreases and increases sharply for large irreversibilities.

Key words: *Poiseuille-Benard channel, Nusselt number, mixed convection, entropy generation*

Introduction

Entropy generation has recently been investigated by many researchers. Bejan [1] studied the entropy minimization in the thermal systems, in addition he analyzed heat transfers from ducts with constant heat flux for flat plates, cylinders in cross flow and rectangular ducts [2-4]. Perez-Blanco [5] integrated the entropy generation rate along the entire surface of the heat

* Corresponding author, e-mail: mfarhadi@nit.ac.ir

exchanger, and then evaluated the effect of the heat transfer augmentation technique on the total entropy-generation rate. Ouellette *et al*. [6] studied the possibility of reductions in the entropy generation (exergy destruction) by using promoters of swirl flow.

Recently, optimal designs of thermal systems have been widely proposed from the viewpoint of thermodynamic Second Law [7-22]. The minimal entropy generation principle has become an important consideration for the heat exchanger design. The optimal design work for rectangular curved ducts based on the minimal entropy generation principle was first reported in recent work of Ko *et al*. [16]. In the study, the entropy generation due to laminar forced convection in a curved rectangular duct with constant wall heat flux was investigated. The optimal Dean number and optimal aspect ratio of duct cross-section according to various relevant design parameters for the rectangular curved duct were analyzed based on minimal entropy generation principle. With numerical methods later, Ko [17] investigated the laminar forced convection and entropy generation in a curved rectangular duct with a single longitudinal rib mounted at midway of the heated wall. The mounted rib with proper sizes was found to result in a significant reduction of entropy generation in the flow field. Through the entropy generation analysis and minimal entropy generation principle, the optimal rib size for the rectangular curved duct with different flow conditions were discussed in detail. Abbassi *et al*. [23] studied entropy generation in Poiseuille-Benard channel flow. He found that the maximum entropy generation is localized at areas where heat exchanged between the walls and the flow is maximum. No significant entropy production is seen in the main flow.

The present study reports a numerical study of Nusselt number and entropy generation in the Poiseuille-Benard channel flow in different angles. By using η, the rate of Nusselt number to the entropy generation, the optimum angle is distinguished for less generated entropy and high Nusselt number. The investigation is carried out from the numerical solutions of complete Navier-Stokes and energy equations by finite volume method. During this study Reynolds, Rayleigh, and Peclet numbers are fixed at Re = 10, Ra = 10^4, and Pe = 20/3 whereas channel angle θ and irreversibility φ are varied from –25 to 30 and from 10^{-5} to 1, respectively.

Governing equation

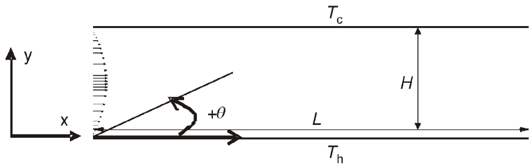

Figure 1. Geometry of the problem

Poiseuille-Benard flow is a channel under a vertical temperature gradient as indicated in fig. 1. Since the Reynolds number is fixed at a weak value, Rayleigh number is at high values, convective rolls appear in the channel alternatively near the lower and the upper walls. In this study the flow is laminar, incompressible and the Boussinesq approximation has been used for buoyancy force effect. Consequently, continuity, momentum, and energy equations can be expressed in the following form in the Cartesian co-ordinate system:

$$\frac{\partial u}{\partial x} \quad \frac{\partial v}{\partial y} \quad 0 \tag{1}$$

$$\frac{\partial u}{\partial \tau} \quad u\frac{\partial u}{\partial x} \quad v\frac{\partial u}{\partial y} \quad \frac{\partial P}{\partial x} \quad \frac{1}{\mathrm{Re}} \quad \frac{\partial^2 u}{\partial x^2} \quad \frac{\partial^2 u}{\partial y^2} \tag{2}$$

$$\frac{\partial v}{\partial \tau} \quad u\frac{\partial v}{\partial x} \quad v\frac{\partial v}{\partial y} \quad \frac{\partial P}{\partial y} \quad \frac{1}{\mathrm{Re}} \quad \frac{\partial^2 v}{\partial x^2} \quad \frac{\partial^2 v}{\partial y^2} \quad \frac{\mathrm{Ra}}{\mathrm{Re\,Pe}}T^* \tag{3}$$

$$\frac{\partial T^*}{\partial \tau} \quad u\frac{\partial T^*}{\partial x} \quad v\frac{\partial T^*}{\partial y} \quad \frac{1}{\mathrm{Pe}} \quad \frac{\partial^2 T^*}{\partial x^2} \quad \frac{\partial^2 T^*}{\partial y} \tag{4}$$

The thermal heat flux exchanged between the walls and the flow is specified by the space-averaged Nusselt number and is calculated as:

$$\overline{\mathrm{Nu}} \quad \frac{1}{\frac{L}{H}} \, {}_{0}^{L/H}\mathrm{Nu}\,\mathrm{d}x \tag{5}$$

where Nu is the local Nusselt number defined as:

$$\mathrm{Nu} \quad \left|\frac{\partial T^*}{\partial n}\right| \tag{6}$$

The space- and time-averaged Nusselt number is defined as:

$$\langle\overline{\mathrm{Nu}}\rangle \quad \frac{1}{t_1} \, {}_{0}^{t_1}\overline{\mathrm{Nu}}\,\mathrm{d}t \tag{7}$$

where t_1 is the total time, whereas Abbassi [23] calculated the $\langle\overline{\mathrm{Nu}}\rangle$ in the period of oscillations of the space-averaged Nusselt number $\langle\overline{\mathrm{Nu}}\rangle$, but in this study, it can not be done because in some angles the variations of Nusselt numbers are not periodic. After the velocity and temperature distributions of the flow field are solved the non-dimensional volumetric entropy generation due to heat transfer irreversibility ($s_{\text{heat transfer}}$) and fluid frictional irreversibility ($s_{\text{fluid friction}}$) can be calculated by the following equations [23]:

$$s_{\text{heat transfer}} \quad \frac{\partial T^*}{\partial x}^{2} \quad \frac{\partial T^*}{\partial y}^{2} \tag{8}$$

$$s_{\text{fluid friction}} \quad \varphi \; 2 \quad \frac{\partial u}{\partial x}^{2} \quad \frac{\partial v}{\partial y}^{2} \quad \frac{\partial u}{\partial y} \quad \frac{\partial v}{\partial x}^{2} \tag{9}$$

where T^*, x, y, u, and v are the dimensionless temperature, Cartesian co-ordinates, and velocity components, respectively, and φ is the irreversibility distribution ratio:

$$\varphi \quad \frac{\mu T_\mathrm{o}}{k} \quad \frac{u_\mathrm{av}}{\Delta T}^{2} \tag{10}$$

where $\Delta T = (T_\mathrm{h} - T_\mathrm{c})$ and $T_\mathrm{o} = (T_\mathrm{h} + T_\mathrm{c})/2$ is defined as bulk temperature. The total entropy generation can be obtained by:

$$s = s_{\text{heat transfer}} + s_{\text{fluid friction}} \tag{11}$$

The dimensionless total entropy generation is calculated by integrating eq. (11):

$$S_\mathrm{g} \quad S_\mathrm{T} \quad S_\mathrm{f} \quad {}_{0}^{1}\,{}_{0}^{L/H} s\,\mathrm{d}x\,\mathrm{d}y \tag{12}$$

where S_T and S_f are the total entropy generation due to the heat transfer and fluid friction, respectively. The time-averaged total entropy generation can be defined as:

$$\langle S_g \rangle \quad \frac{1}{t_1} \int_0^{t_1} S_g \,\mathrm{d}t \tag{13}$$

The Bejan number (Be) which describes the contribution of heat transfer entropy on overall entropy generation is defined by:

$$\mathrm{Be} \quad \frac{\langle S_{\text{heat transfer}} \rangle}{\langle S_g \rangle} \tag{14}$$

The Be ranges from 0 to 1. When Be 1/2 the irreversibility due to heat transfer dominates, while for Be 1/2 the irreversibility due to viscous effects dominates. For Be 1/2, the entropy generation rates from heat transfer and fluid friction are equal.

Computational domain and boundary condition

In this study, the flow is supposed to be laminar and two-dimensional in addition the length and width of channel is supposed to 10 and 1, respectively. For turning the channel, θ is positive and negative for clock wise and *vice versa*, respectively. At the channel inlet a fully developed parabolic profile for the axial velocity is prescribed:

$$u \quad 1.5 \; 1 \quad \left(\frac{Y}{Y_B}\right)^2, \quad v \quad 0 \tag{14}$$

where $Y_b = H/2$. The components of dimensionless velocity in Cartesian co-ordinates at channel inlet can be evaluated as:

$$\begin{aligned} u &\quad |V|\cos\theta \\ v &\quad |V|\sin\theta \end{aligned} \tag{15}$$

where θ is the channel angle and V is defined as:

$$|V| \quad \sqrt{u^2 \quad v^2} \tag{16}$$

On all solid walls, if there is no flow through the wall, convective fluxes of all quantities are zero and the diffusive fluxes in the momentum equations at walls are replaced by the shear force [24]. To avoid discontinuity, the temperature of incoming stream is supposed to change linearly from T_h at the bottom wall to T_c at the upper wall. At outlet the convective boundary condition (CBC) is used that is formulated as:

$$\frac{\partial \phi}{\partial t} \quad u_{av} \frac{\partial \phi}{\partial X} \quad 0 \tag{17}$$

where ϕ is any dependent variable and u_{av} is the average velocity at the inlet of the channel.

Numerical procedure and validation

The mentioned equations in pervious section were solved by UTFN code [24]. This code uses finite volume method and SIMPLE algorithm for discretizing the governing equations of flow and resolving the pressure-velocity coupling system. In addition, all the variables are stored in same nodes by using collocated grid. The convection and diffusion term of the equations are discretized by central difference scheme (CDS). More detail of these techniques is available in refs. [24, 25]. The Poiseuille-Benard channel has been studied by some researchers. For validation of this code, a Poiseuille-Benard channel with the length of 20, width of 1 at Re =10 and Ra = 10^4 was solved. The non-uniform grid is used and the study of grid dependence indicated in tab. 1 shows that a non-uniform grid of 200 30 is sufficient to obtain accurate results. The results from this code and other references are reported in tab. 2. This table shows that there are good agreement between the results of this program and the previous studies. So that the maximum difference at Nusselt number and dimensionless period (Θ) are 3.37% and 6.52% in [27] and [28], respectively.

Table 1. Grid dependence

Grid	150 20	200 30	250 40
$\langle\overline{\mathrm{NU}}\rangle$	2.327	2.487	2.531

Table 2. Poiseuille-Benard channel flow: Re = 10, Pe = 20/3, and Ra = 10^4

Reference	Present study	Ref. [26]	Ref. [27]	Ref. [28]
Period$^{\Theta}$	1.304	1.273	1.332	1.395
$\langle\overline{\mathrm{NU}}\rangle$	2.487	2.536	2.574	2.558

Results and discussion

Fluid flow

The streamline for Poiseuille--Benard channel θ = 0 at in an instant is depicted in fig. 2. It is clear from fig. 2 that the values of temperature and velocity components fluctuate periodically along the channel. That is because of small Re number and large value of Ra number.

Figure 2. Instantaneous streamlines for Poiseuille-Benard channel at angle θ = 0

When θ is not equal to zero, the size of vortexes in vicinity of the walls change that is due to the gravity force on fluid. When θ < 0, by increasing θ gradually large vortexes appear in the vicinity of the bottom wall because of the increase in the fluid velocity. Finally at θ = –25, large recalculating zone will be formed along the channel (fig. 3a).

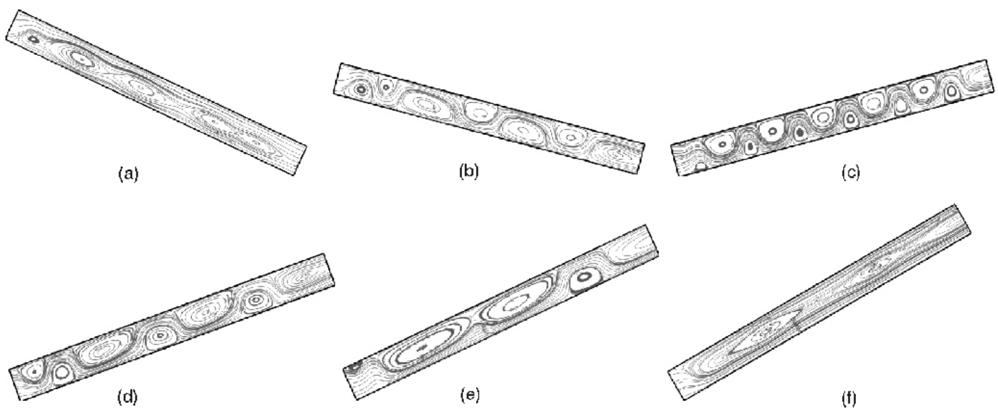

Figure 3. Instantaneous streamlines for orientation angle θ
(a) –25, (b) –15, (c) 15, (d) 20, (e) 25, and (f) 30 at time unit =140

In case of $\theta > 0$, vortexes generated in the vicinity of the top wall will be larger, while θ increases. Finally at $\theta = 30$, a large recalculating zone appears along the top wall, fig. 3(e). Angles of 25, 30, and –25 are called the critical angle because at these angles some large recirculating zones will be generated along the channel (fig. 3).

Heat transfer

It is expected that the Nusselt number variation along the channel changes periodically by periodic change of temperature along the channel. The starting time $t = 0$ in this study is the instant when the averaged Nusselt number at the bottom wall ($\overline{\mathrm{Nu}}_b$) is maximum. As it is mentioned in the pervious section, the way of vortex formation in the vicinity of the hot and cold walls at $\theta < 0$ and $\theta > 0$ are opposite. Therefore, in the rest, we only consider the $\overline{\mathrm{Nu}}_b$. Figure 4 presents the $\overline{\mathrm{Nu}}_b$ variation in respect to time at different angles.

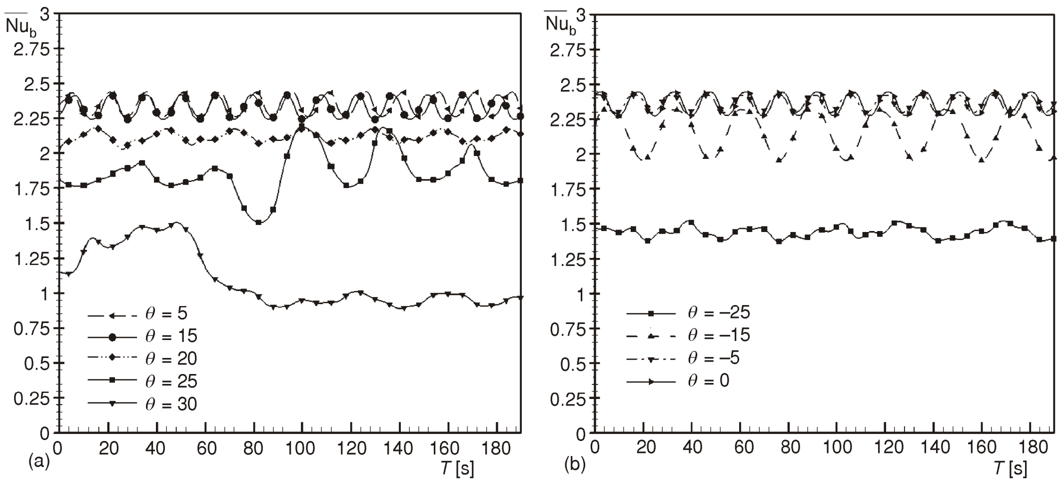

Figure 4. Variation of the $\overline{\mathrm{Nu}}_b$ in respect to time at (a) positive and (b) negative angles θ

It can be concluded that the variation of $\overline{\mathrm{Nu}}_b$ along the time is periodic and it will be transposition with respect to the case of $\theta = 0$. It is due to the approximately same vortexes which are generated besides of the channel walls. At two studied angles, $\theta = 20$ and –15, the Nusselt number variations are not same. At $\theta = 20$ the smaller vortexes appear along the bottom wall, therefore, the $\overline{\mathrm{Nu}}_b$ variations are periodic with the small amplitude but at $\theta = -15$, these variations are periodic with high amplitude as results of large vortex formation in vicinity of bottom wall. At the critical angles, the variation of $\overline{\mathrm{Nu}}_b$ are not periodic due to generation of large reticulating region along the channel.

Figure 5 shows the variation $\overline{\mathrm{Nu}}_b$ the instantaneous local Nusselt number at different angles along the channel walls. It can be seen that the variations of Nu_b and Nu_t *vs.* the channel length are completely periodic at most of the studied angles but at critical angles, these variations are chaos. It is due to the flow field and form of the created vortexes in the channel. Time and space averaged Nusselt number variation at different angles is shown in fig. 6. It can be observed that $\langle\overline{\mathrm{Nu}}\rangle$ at critical angles decreases sharply and it is approximately constant for 10 θ –5.

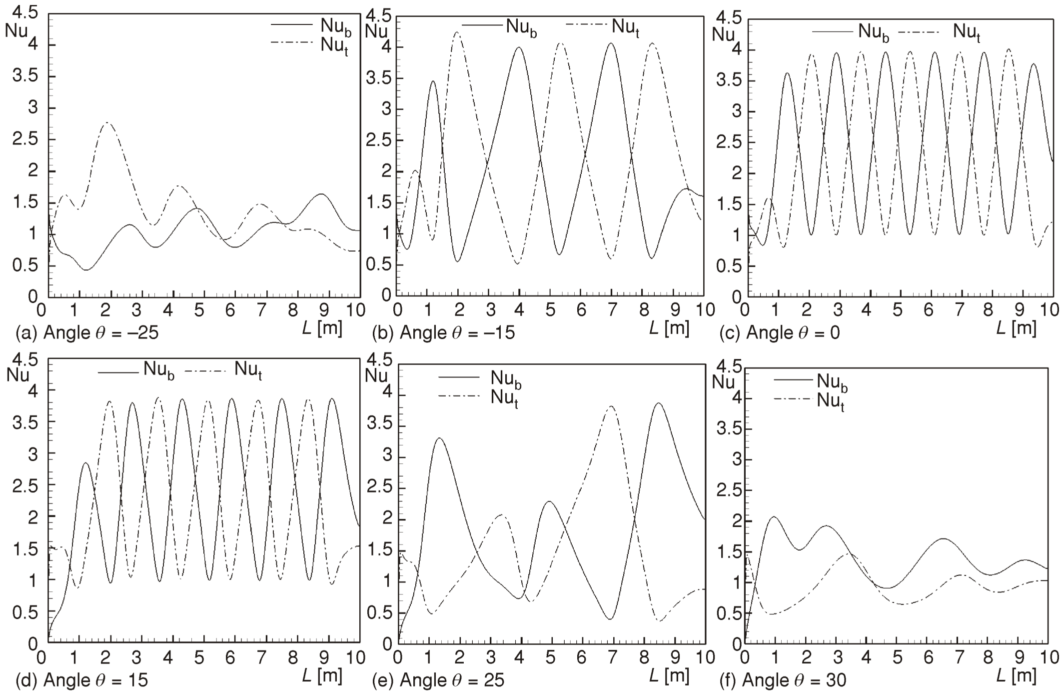

Figure 5. Instantaneous variation of the local Nusselt number along the channel walls at different angles θ

Entropy generation

From eqs. (8) to (11), it can be understood that the value of entropy generation in flow field is depended on irreversibility, temperature, and velocity gradients. When irreversibility is very small, the entropy generated due to heat transfer has a predominant effect on the S_g.

Figure 7 shows the variation of S_g at different angles in respect to time when irreversibility is very small ($\varphi = 10^{-3}$). It can be seen that as far as φ is very small, the behavior of S_g variations are same as $\overline{Nu}_b$ variations. It means that when $\overline{Nu}_b$ changes periodic, S_g has also periodic changed but with different frequency. Figure 8 presents $\overline{Nu}_b$ and S_g variations at $\theta = 0$ for $\varphi = 10^{-3}$. It can be observed that in one oscillation of $\overline{Nu}_b$, the total entropy generation has two maximums and two minimums. These results are in a very good agreement with Abbassi *et al*. [23].

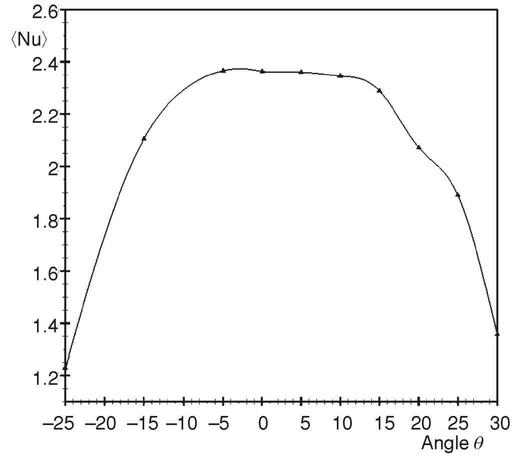

Figure 6. Time and space averaged Nusselt number variations at different angles θ

The instantaneous contours of the Bejan number (Be) are shown in fig. 9 for different angles. The variation of time averaged of total entropy generation and Be number at different

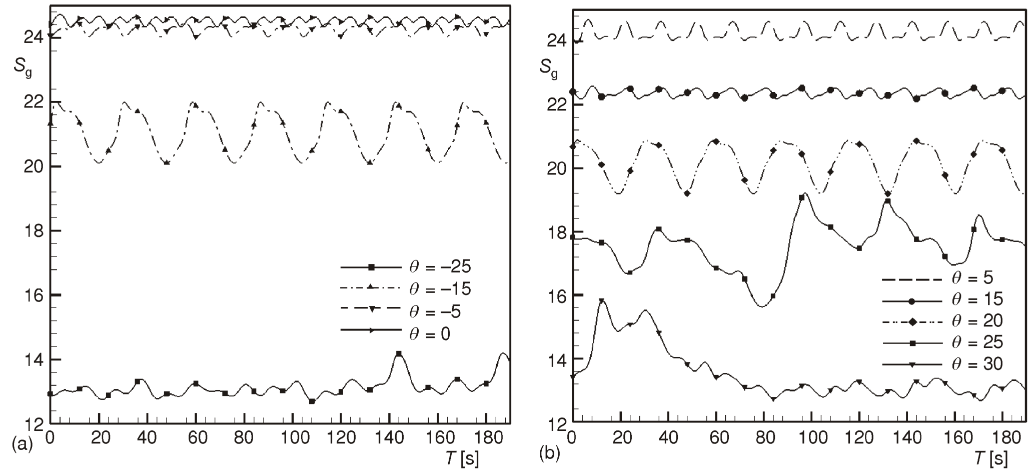

Figure 7. Variation of S_g at different angles θ in respect to time at small irreversibility for $\varphi = 10^{-3}$

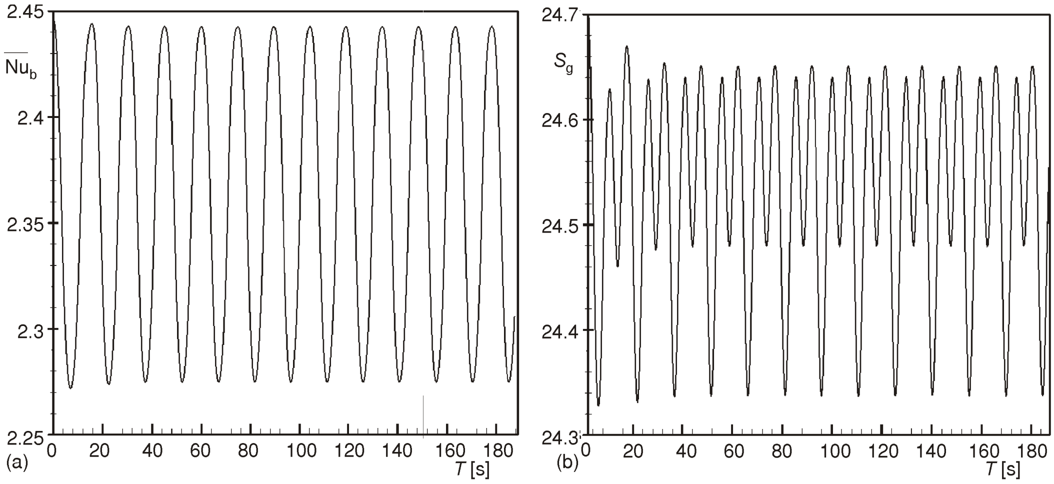

Figure 8. $\overline{\mathrm{Nu}}_b$ and S_g variations at angle $\theta = 0$ for $\varphi = 10^{-3}$

angles are depicted at fig. 10 when $\varphi = 10^{-3}$. From fig. 9 it can be concluded that the entropy generation due to heat transfer has predominant effect on S_g in vicinity of walls where the heat exchanged between wall and fluid is maximum and in vortex centers the velocity gradients are high so the effect of the fluid friction is more important.

In fig. 10, $\langle S_g \rangle$ vary same as $\langle S_T \rangle$ because the irreversibility is very small so that the total entropy generation decreases sharply at critical angles.

It is because at these angles some large vortexes appear along the channel length consequently the heat exchanged between the walls and fluid decrease. In addition, the Be number decreases because at critical angles the effect of $\langle S_f \rangle$ on $\langle S_g \rangle$ is more than other angles. By increasing irreversibility φ, the entropy generation at critical angles will be higher than other angles (fig. 11) and the Be number goes to zero (fig. 12).

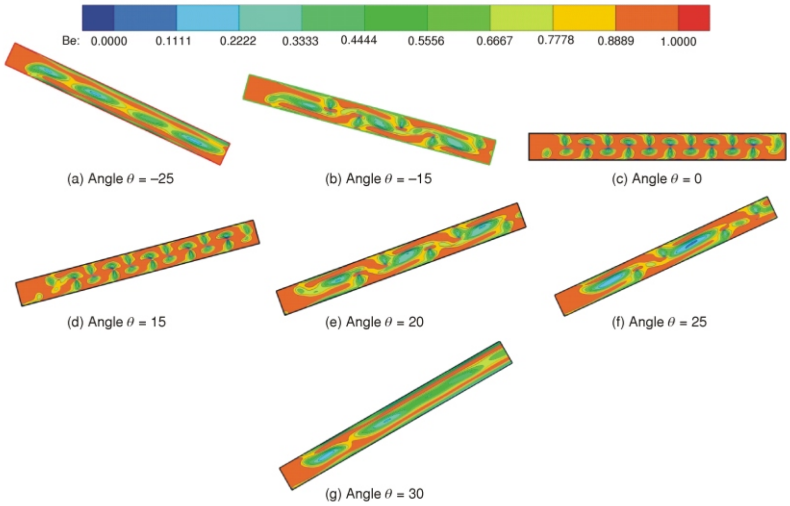

Figure 9. Instantaneous contours of Bejan number at different angles θ at time unit =140 (color image see on our web site)

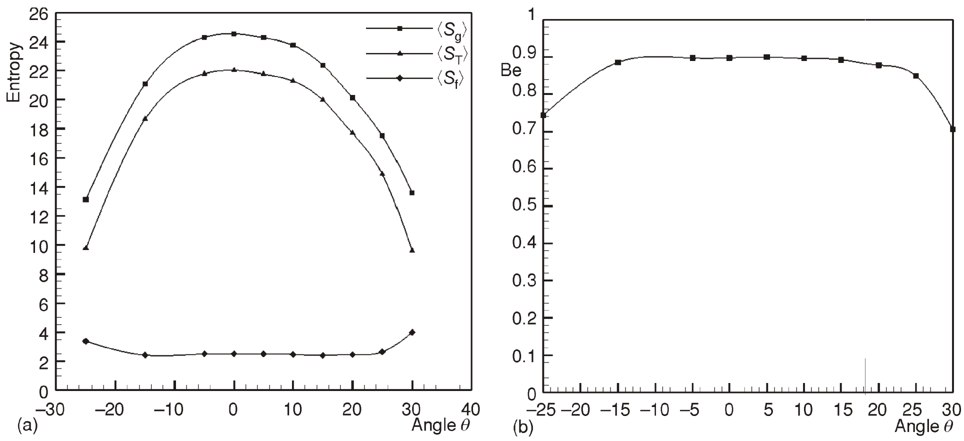

Figure 10. Variation of time and space averaged of (a) entropy generation and (b) Be number with angle θ at $\varphi = 10^{-3}$

Optimization

In this study optimal angle for a specific φ is defined as function of optimization factor which introduce bellow:

$$\eta \quad \frac{\langle \overline{\mathrm{Nu}} \rangle}{\langle S_{\mathrm{g}} \rangle} \tag{18}$$

Considering the η, optimum angle is an angle which the division of heat transfer to total entropy generation is at maximum value. Optimization factor is presented in fig. 13 for different value of irreversibility. While φ increases, the value of η decreases and η is approximately constant except at critical angles. When the irreversibility is very small, it can be found a

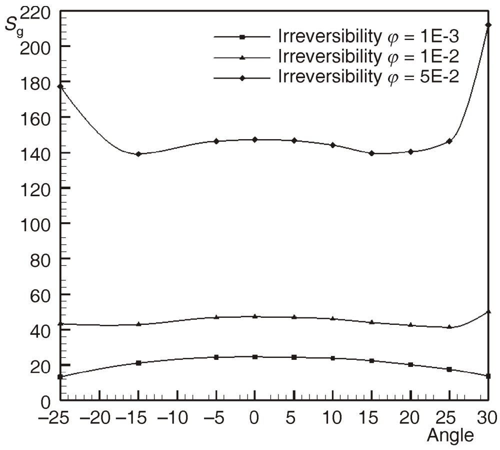

Figure 11. Variation of time and space averaged of entropy generation with angle θ at different irreversibility φ

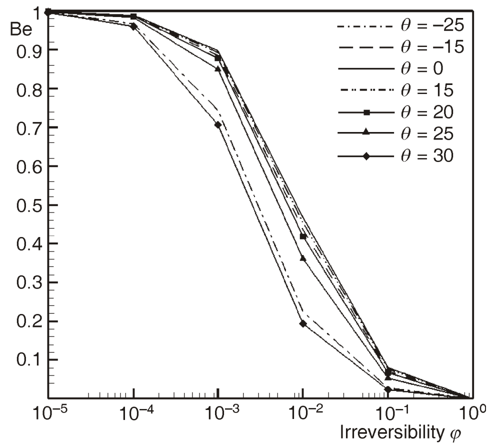

Figure 12. Variation of time and space averaged Be number with irreversibility φ at different angles θ

maximum for η and can be defined the optimal angle. For example by assuming $\varphi = 10^{-3}$, although $\langle\overline{\text{Nu}}\rangle$ is at maximum value at $-5 < \theta < 5$ (see fig. 6), but the entropy generation at this angles is more than other angles. By using the η the optimum angle can be found at $15 < \theta < 20$. In these angles the percentage reduction of the Nusselt number in comparison with the maximum value of the Nusselt number are from 3.23% to 12.4%. On the other hand, entropy generation shows the reduction from 8.83% to 18.11% for these angles. As a result, the optimization factor can be derived from angle θ= 15 to θ = 20. Optimization factor can be used for finding optimal angle in this geometry where irreversibility is small.

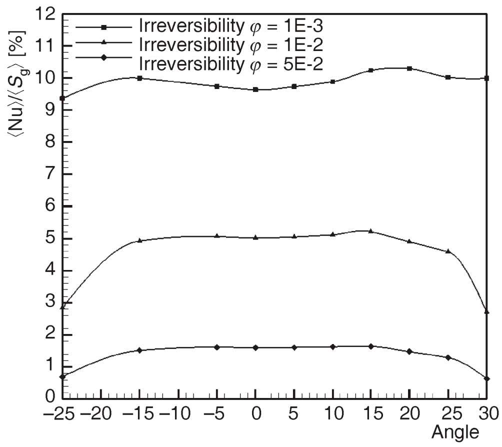

Figure 13. Variation of η with angle θ at different irreversibility φ

Conclusions

The variations of entropy generation and Nusselt number in 2-D laminar Poiseuille-Benard channel flow in different angels have been studied numerically. Moreover the optimum angle for a specific φ is defined by optimization factor (η). Reynolds, Peclet, and Rayleigh numbers were fixed at Re = 10, Pe = 20/3, and Ra = 10^4 whereas irreversibility φ and channel angle θ are changed from 10^{-5} to 1 and from –25 to 30, respectively. According to the results obtained, the following conclusion are achieved.

Vortex generated along the channel are approximately at the same size when the slope of the channel is small but by nearing to critical angles, the vortexes are not same and finally, large vortexes appear along the channel at critical angles.

Time and space averaged Nusselt number will not change at small value of θ but it decreases sharply at critical angles.

Entropy generation due to heat transfer is largely higher near the channel walls than that in the central flow, where as the entropy generation due to fluid friction is largely higher in the central flow especially in the vortex centers. When irreversibility is small, S_T has more effect on S_g in comparison with S_f, therefore, S_g will decreases at critical angles. When irreversibility is large, S_f has more effect on S_g in comparison with S_T and S_g increases at critical angles because large recalculating region appears along the channel and then, S_f will increase.

Nomenclature

Be – Bejan number ($= S_T/S_g$), [–]
C_f – specific heat at constant pressure, [$m^2s^{-2}K^{-1}$]
g – gravitational acceleration, [ms^{-2}]
H – channel width, [m]
K – thermal conductivity of fluid, [$kgms^{-3}K^{-1}$]
L – length of the channel, [m]
Nu – local Nusselt number, [–]
Nu_b – local Nusselt number at the bottom wall, [–]
Nu_t – local Nusselt number at the top wall, [–]
$\overline{Nu}$ – space averaged Nusselt number, [–]
$\langle Nu \rangle$ – space and time-averaged Nusselt number, [–]
P – dimensionless pressure ($= P/\rho_{av}^2$), [–]
Pe – Peclet number (= RePr), [–]
Pr – Prantel number ($= mC_p/K$), [–]
Ra – Rayleigh number [$= \rho g \beta (T_h - T_c) H^3/\alpha \nu$], [–]
Re – Reynolds number [$= u_{av}H/\nu$], [–]
S_g – volumetric non-dimensional entropy generation, [–]
$\langle S_g \rangle$ – dimensionless time averaged total entropy generation, [–]
T – temperature, [K]
T^* – dimensionless temperature [$= (T - T_c)/(T_h - T_c)$], [–]
u_{av} – average u-component at the channel inlet, [ms^{-1}]
u, v – dimensionless velocity components [$= U_x/u_{av}, U_y/u_{av}$], [–]
U_x, U_y – local velocity components in X, Y – co-ordinate, [ms^{-1}]
x, y – dimensionless Cartesian co-ordinates [$= X/H, Y/H$], [–]
X, Y – local Cartesian co-ordinate, [m]

Greek letters

β – thermal expansion coefficient, [K^{-1}]
Θ – dimensionless period, [–]
θ – orientation angle, [°]
φ – irreversibility distribution ratio, [–]
μ – dynamic viscosity of the fluid, [$kgm^{-1}s^{-1}$]
ν – kinematic viscosity of the fluid, [m^2s^{-1}]
ρ – density of the fluid, [kgm^{-3}]
τ – dimensionless time ($= tu_{av}/H$), [–]

Subscripts

c – cold
h – hot
av – average
w – wall

References

[1] Bejan, A., A Study of Entropy Generation in Fundamental Convective Heat Transfer, *ASME, J. Heat Transfer, 101* (1979), 4, pp. 718-725
[2] Bejan, A., Second-Law Analysis in Heat Transfer, *Energy, 5* (1980), 8-9, pp. 721-32
[3] Bejan, A., Second-Law Analysis in Heat Transfer and Thermal Design, *Adv. Heat Transfer, 15* (1982), 1, pp. 1-58
[4] Bejan A., Fundamentals of Exergy Analysis, Entropy-Generation Minimization, and the Generation of Flow Architecture, *International Journal of Energy Research, 26* (2002), 7, pp. 545-565
[5] Perez-Blanco, H., Irreversibility in Heat-Transfer Enhancement, in: Second Law Aspects of Thermal Design, *ASME, Heat Transfer Division, 33* (1984), pp. 19-26
[6] Ouellette, W. R., Bejan, A., Conservation of Available Work (Exergy) by Using Promoters of Swirl Flow in Forced Convection Heat-Transfer, *Energy, 5* (1980), 7, pp. 587- 596

[7] Bejan, A., Entropy Generation Minimization, CRC Press, Boca Raton, Fla., USA, 1996
[8] Bejan, A., Entropy Generation through Heat and Fluid Flow, John Wiley and Sons, New York, USA, 1982
[9] Nag, P. K., Kumar, N., Second Law Optimization of Convection Heat Transfer through a Duct with Constant Heat Flux, *International Journal of Energy Research, 13* (1989), 5, pp. 537-543
[10] Sahin, A. Z., Irreversibilities in Various Duct Geometries with Constant Wall Heat Flux and Laminar Flow, *Energy, 23* (1998), 6, pp. 465-473
[11] Sahin, A. Z., Thermodynamics of Laminar Viscous Flow through a Duct Subjected to Constant Heat Flux, *Energy, 21* (1996), 12, pp. 1179-1187
[12] Shuja, S. Z., Optimal Fin Geometry Based on Exergoeconomic Analysis for a Pin-Fin Array with Application to Electronics Cooling, *Exergy, 2* (2002), 4, pp. 248 58
[13] Sara, O. N, *et al*., Secondary Law Analysis of Rectangular Channels with Square Pin-Fins, *Int. Comm. Heat Mass Transfer, 28* (2001), 5, pp. 617-630
[14] Ko, T. H., Ting, K., Entropy Generation and Thermodynamic Optimization of Fully Developed Laminar Convection in a Helical Coil, *Int. Comm. Heat Mass Transfer, 32* (2005), 1-2, pp. 214-223
[15] Ko, T. H., Analysis of Optimal Reynolds Number for Developing Laminar Forced Convection in Double-Sine Ducts Based on Entropy Generation Minimization Principle, *Energy Conversion and Management, 47* (2006), 6, pp. 655-670
[16] Ko, T. H., Ting, K., Entropy Generation and Optimal Analysis for Laminar Forced Convection in Curved Rectangular Ducts: A Numerical Study, *International Journal of Thermal Sciences, 45* (2006), 2, pp. 138-150
[17] Ko, T. H., Numerical Investigation on Laminar Forced Convection and Entropy Generation in a Curved Rectangular Duct with Longitudinal Ribs Mounted on Heated Wall, *International Journal of Thermal Sciences, 45* (2006), 4, pp. 390-404
[18] Ko, T. H., Ting, K., Optimal Reynolds Number for the Fully Developed Laminar Forced Convection in a Helical Coiled Tube, *Energy, 31* (2006), 12, pp. 2142-2152
[19] Ko, T. H., Thermodynamic Analysis of Optimal Curvature Ratio for Fully Developed Laminar Forced Convection in a Helical Coiled Tube with Uniform Heat Flux, *International Journal of Thermal Sciences, 45* (2006), 7, pp. 729-737
[20] Ko, T. H., Numerical Investigation on Laminar Forced Convection and Entropy Generation in a Helical Coil with Constant Wall Heat Flux, *Numerical Heat Transfer, Part A, 49* (2006), 3, pp. 257-278
[21] Ko, T. H., Numerical Analysis of Entropy Generation and Optimal Reynolds Number for Developing Laminar Forced Convection in Double-Sine Ducts with Various Aspect Ratios, *International Journal of Mass and Heat Transfer,49* (2006), 3-4, pp. 718-726
[22] Narusawa, U., The Second-Law Analysis of Mixed Convection in Rectangular Ducts, *Heat Mass Transfer, 37* (2001), 2-3, pp. 197-203
[23] Abbassi, H, Magherbi, M., Brahim , A. B., Entropy Generation in Poiseuille-Benard Channel Flow, *International Journal of Thermal Sciences, 42* (2003), 12, pp. 1081-1088
[24] Nourollahi, M., Generation of CFD Code for Solving the Fluid Governing Equations in Non-Orthogonal co-ordinate Systems, M. Sc. thesis, Faculty of Mechanical Engineering, Babol Noshirvani University of Technology, Babol, Iran, 2007
[25] Ferziger, J., H., Peric, M., Computational Methods for Fluid Dynamics, Springer-Verlag, Berlin, Heidelberg, New York, USA, 2002
[26] Comini, G., Manzan, M., Cortella, G., Open Boundary Conditions for the Stream Function of Unsteady Laminar Convection, *Numerical Heat Transfer, Part B, 31* (1997), 2, pp. 217-234
[27] Evans, G., Paolucci, S., The Thermoconvective Instability of Plane Poiseuille Flow Heated from below: A Benchmark Solution for Open Boundary Flow, *International Journal Numerical Method in Fluids, 11* (1990), 7, pp. 1001-1013
[28] Abbassi, H., Turki, S., Nasrallah, S., B., Numerical Investigation of Forced Convection in a Plane Channel with a Built-in Triangular Prism, *International Journal of Thermal Sciences, 40* (2001), 7, pp. 649-658

Paper submitted: July 30, 2008
Paper revised: May 24, 2009
Paper accepted: July 27, 2009